ARL-TR-7450 ● SEP 2015

US Army Research Laboratory

Scattering From the Finite-Length, Dielectric Circular Cylinder: Part II – On the Validity of an Analytical Solution for Characterizing Backscattering from Tree Trunks at P-Band

by DaHan Liao

NOTICES

Disclaimers

The findings in this report are not to be construed as an official Department of the Army position unless so designated by other authorized documents.

Citation of manufacturer's or trade names does not constitute an official endorsement or approval of the use thereof.

Destroy this report when it is no longer needed. Do not return it to the originator.

ARL-TR-7450 ● SEP 2015

US Army Research Laboratory

Scattering From the Finite-Length, Dielectric Circular Cylinder: Part II – On the Validity of an Analytical Solution for Characterizing Backscattering from Tree Trunks at P-Band

by DaHan Liao
Sensors and Electron Devices Directorate, ARL

REPORT DOCUMENTATION PAGE

Form Approved
OMB No. 0704-0188

1. REPORT DATE *(DD-MM-YYYY)*	2. REPORT TYPE	3. DATES COVERED (From - To)
Sep 2015	Final	2014–2015

4. TITLE AND SUBTITLE

Scattering From the Finite-Length, Dielectric Circular Cylinder: Part II – On the Validity of an Analytical Solution for Characterizing Backscattering from Tree Trunks at P-Band

5a. CONTRACT NUMBER

5b. GRANT NUMBER

5c. PROGRAM ELEMENT NUMBER

6. AUTHOR(S)

DaHan Liao

5d. PROJECT NUMBER

5e. TASK NUMBER

5f. WORK UNIT NUMBER

7. PERFORMING ORGANIZATION NAME(S) AND ADDRESS(ES)

US Army Research Laboratory
ATTN: RDRL-SER-U
2800 Power Mill Road
Adelphi, MD 20783-1138

8. PERFORMING ORGANIZATION REPORT NUMBER

ARL-TR-7450

9. SPONSORING/MONITORING AGENCY NAME(S) AND ADDRESS(ES)

10. SPONSOR/MONITOR'S ACRONYM(S)

11. SPONSOR/MONITOR'S REPORT NUMBER(S)

12. DISTRIBUTION/AVAILABILITY STATEMENT

Approved for public release; distribution unlimited.

13. SUPPLEMENTARY NOTES

14. ABSTRACT

A comprehensive set of simulations is performed to analyze the accuracy of an analytical solution for characterizing the backscattering responses of circular cylindrical tree trunks located above a dielectric ground. The formulation of interest here is from the volumetric current integration method, combined with a ray-based approach for the treatment of ground effects. Through comparisons with a reference solution provided by a full-wave solver, the region of validity of the closed-form approximate solution as functions of trunk length, trunk radius, incidence angle, and polarization is derived. Trunks with and without tapering along their lengths are considered. It is noted that in general the error behavior of the vertical-vertical (vv) solution exhibits more complexity compared to that of the horizontal-horizontal (hh) solution, due to the Brewster angle effects of the trunk and the ground; consequently, the hh solution is valid over a wider range of length and radius values. The backscattering signatures of the trunks are also examined in the imaging domain. It is found that the analytical solution can correctly predict the single ground-bounce returns but may not consistently capture other less prominent effects such as scattering from the top of the trunk and higher-order interactions.

15. SUBJECT TERMS

Analytical solution, discrete scatterer model, electromagnetic scattering, foliage-penetration radar, tree trunk scattering

16. SECURITY CLASSIFICATION OF:			17. LIMITATION OF ABSTRACT	18. NUMBER OF PAGES	19a. NAME OF RESPONSIBLE PERSON
a. REPORT	b. ABSTRACT	c. THIS PAGE			DaHan Liao
Unclassified	Unclassified	Unclassified	UU	36	19b. TELEPHONE NUMBER (Include area code) (301) 394-1741

Contents

List of Figures

INTENTIONALLY LEFT BLANK.

1. Introduction

Understanding the scattering behaviors of trees plays a critical role in determining the performance of foliage-penetration radar systems. The foliage-penetration radar modality of interest in this study consists of an airborne sensing system that illuminates a scene with a low frequency signal (typically, at low-grazing angles), and then measures the backscattered responses in the far field. Subsequently, the detection and surveillance of ground targets obscured by the trees can be carried out with various clutter cancellation, moving target indication, and synthetic aperture radar imaging processing methods. In the low frequency region, in terms of the scattering effects, the contributions from the leaves and small branches are often assumed to be negligible; and while the inclusion of the contributions from large branches can modify the overall response to an extent, the most salient scattering features in the backscattering direction are generated primarily by the tree trunks.[1] Characterizing the electromagnetic responses of the tree trunks, then, constitutes an integral part of the detection algorithm development and radar performance evaluation process.

Although full-wave simulations of large forest scenes have been carried out in previous studies,[1,2] numerical solutions are rather computationally intensive. An analytical approach is not only advantageous in computational efficiency, but also in providing a more satisfying physical interpretation of the scattering effects. In accordance to the discrete scatterer approach,[3] a tree trunk can be treated as a finite-length, dielectric circular cylinder, the scattering solution of which can be obtained with approximate analytical methods such as surface current integration or volumetric current integration.[4–8] (Note that a physical optics technique can also be applied, but such an approach is more appropriate at the higher frequency region. For the range of parameters of interest here, the radii of curvature of the trunks are not always large compared to the wavelength.) The surface current integration method exploits the supposition that the surface fields of the finite-length cylinder are the same as those of the infinite-length case, whereas the volumetric current integration method makes a similar assumption but for the internal fields.[4,6] With the stated approximation, the scattering matrix elements of the finite-length structure can then be calculated using the equivalence principle. The validity of both methods has been investigated in previous studies for scatterers in free space.[7,9,10]

The focus of the current work is on the volumetric current-based approach, since it has been shown that this method is more accurate relative to the surface current-based one.[7] Detailed derivations of the relevant formulations are discussed in Part I of this study.[8] However, a comprehensive evaluation of the accuracy of this

method for scatterers located above a dielectric ground has not been presented. As such, this work is organized as follows. In Section 2, an overview of the analytical formulations for the scattering of a tree trunk located above a dielectric ground is put forth. In Section 3, the region of validity of the closed-form backscattering solution as functions of trunk length, trunk radius, incidence angle, polarization, and trunk tapering is deduced by comparing the results with those from a full-wave solution; the responses are also examined in the imaging domain to elucidate the relevancy of various scattering mechanisms. Finally, in Section 4, a summary of the work is given.

2. Analytical Solution

As discussed in Part I of this study,[8] a particular closed-form solution for the scattering from the finite-length, dielectric circular cylinder (with length L and radius a) in free space can be obtained by approximating the internal fields of the cylinder as those of the infinite-length case. A scattering matrix can be subsequently constructed with an application of the volumetric equivalence principle by propagating the fields radiated by the electric polarization current inside the cylindrical structure. As pointed out by Lang and de Matthaeis,[7,10] such a solution is reasonably accurate in the forward scattering cone, and the accuracy improves with increasing cylinder length, for a given radius. Note that by integrating over a finite cylindrical volume, this method somewhat implicitly includes the scattering from the ends of the finite-length structure; however, this scattering component may not be captured accurately. Here, the overall solution above is referred to as the volumetric current integration method, and the relevant formulations from Part I of this study are tabulated in the Appendix. For the case when the tree trunk is located above a finite-conducting ground (with the air–ground interface at $z = 0$), a total scattering matrix can be constructed with a multi-ray approach by coherently summing the direct wave and the ground-reflected waves. Succinctly, the total scattering matrix—expanded into its first 4 main contributions—can be written as[8,12]

$$\begin{aligned}\overline{\overline{S}}\left(\hat{k}_s,\hat{k}_i\right) = {} & \overline{\overline{S}}^{fs}\left(\hat{k}_s,\hat{k}_i\right)e^{-jk_o\left(\hat{k}_i\cdot\vec{r}_o-\hat{k}_s\cdot\vec{r}_o\right)} + \overline{\overline{S}}^{fs}\left(\hat{k}_s,\hat{k}_{i,g}\right)\cdot\overline{\overline{\Gamma}}\left(\hat{k}_i\right)e^{-jk_o\left(\hat{k}_i\cdot\vec{r}_g-\hat{k}_s\cdot\vec{r}_o\right)} \\ & + \overline{\overline{\Gamma}}\left(\hat{k}_s\right)\cdot\overline{\overline{S}}^{fs}\left(\hat{k}_{s,g},\hat{k}_i\right)e^{-jk_o\left(\hat{k}_i\cdot\vec{r}_o-\hat{k}_s\cdot\vec{r}_g\right)} + \overline{\overline{\Gamma}}\left(\hat{k}_s\right)\cdot\overline{\overline{S}}^{fs}\left(\hat{k}_{s,g},\hat{k}_{i,g}\right)\cdot\overline{\overline{\Gamma}}\left(\hat{k}_i\right)e^{-jk_o\left(\hat{k}_i\cdot\vec{r}_g-\hat{k}_s\cdot\vec{r}_g\right)},\end{aligned} \tag{1}$$

where $\vec{r}_o$ is the location of the center of the scatterer; $\vec{r}_g = \vec{r}_o - 2\left(\vec{r}_o \cdot \hat{z}\right)\hat{z}$; $\hat{k}_{i,g} = \hat{k}_i - 2\left(\hat{k}_i \cdot \hat{z}\right)\hat{z}$; $\hat{k}_{s,g} = \hat{k}_s - 2\left(\hat{k}_s \cdot \hat{z}\right)\hat{z}$; $\overline{\overline{S}}^{fs}(\cdot,\cdot)$ is the cylinder free space response given in the Appendix; and $\overline{\overline{\Gamma}}\left(\hat{k}_{i,s}\right)$ is the ground reflection coefficient matrix

$$\overline{\overline{\Gamma}}\left(\hat{k}_{i,s}\right) = \begin{bmatrix} r_v\left(\hat{k}_{i,s}\right) & 0 \\ 0 & r_h\left(\hat{k}_{i,s}\right) \end{bmatrix}, \tag{2}$$

with $r_v\left(\hat{k}_{i,s}\right)$ and $r_h\left(\hat{k}_{i,s}\right)$ as the ordinary horizontally and vertically polarized ground reflection coefficients, respectively. The incident and scattered wave directions ($\hat{k}_i$ and $\hat{k}_s$, respectively) and their associated polarization vectors are as defined in the Appendix. The first term in Eq. 1 is the direct wave from the cylinder; the second and third terms correspond to the single ground-bounce returns; and the last term is the double ground-bounce contribution. Note that in the backscattering direction ($\hat{k}_s = -\hat{k}_i$), the dominant response comes from the single ground-bounce returns—that is, from the dihedral effect of the trunk and the ground surface. The formulation in Eq. 1 essentially exploits 3 approximations: first, the trunk volumetric current is estimated as that from the infinite-length cylinder in free space; second, the ground effects on that current are taken as negligible; and finally, the scattering in the presence of the ground is heuristically captured as rays.

In terms of modeling the physical geometry, the above developments assume the tree trunk is a circular cylindrical structure with a constant radius. A more realistic representation is a cylindrical structure that has a varying radius along its length. In fact, most tree trunks in nature have a tapered profile defined by an exponential expansion (or flare) near the base.[11] Accordingly, circular cylinders with and without tapering along their lengths are considered in this work (Fig. 1). Scattering from a tapered trunk is treated by first segmenting the structure into discrete constant-radius subsections along its length; then, the response of each subsection is deduced using Eq. 1; and finally, the total response of the whole structure is calculated by summing the responses of all the subsections.

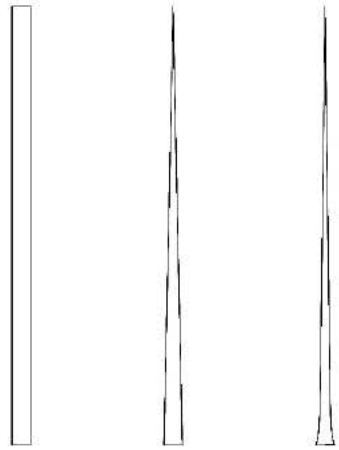

Fig. 1 Trunk profiles considered in this study: a) untapered circular cylindrical trunk, b) linearly tapered circular cylindrical trunk, and c) nonlinearly tapered circular cylindrical trunk. Each structure has base-to-apex height (or length) *L* and base radius *a*.

3. Validation with Full-Wave Solution

The accuracy of the analytical scattering solution for a tree trunk located above a ground is investigated by comparing the backscattering results with those from a finite-difference time-domain (FDTD) solver.[1,13,14] Only the co-polarized returns are considered in this work. (Formally, the backscattered cross-polarized responses are zero for the structures studied here.) In the frequency domain, the average error in the closed-form solution is examined as functions of the trunk length, trunk radius, and incidence angle for 3 different structures—the untapered circular cylindrical trunk, the linearly tapered circular cylindrical trunk, and the nonlinearly tapered circular cylindrical trunk. The average error is defined as

$$\varepsilon_{pp} = \left\langle \left| S^r_{pp}\left(-\hat{k}_i, \hat{k}_i\right)\Big|_{[dB]} - \left| S_{pp}\left(-\hat{k}_i, \hat{k}_i\right)\right|_{[dB]} \right| \right\rangle, \; pp = vv, hh \tag{3}$$

where S^r_{pp} denotes the reference (FDTD) solution, and the averaging operation is performed over the frequency band $\Delta f = [200\,\text{MHz}, 500\,\text{MHz}]$ (P-band) with N_f = 301 frequency points. Trunk profiles with dimensions in the range of $0.1\lambda_c \le L_{\lambda_c} \le 10\lambda_c$ and $0.1\lambda_c \le a_{\lambda_c} \le \lambda_c$ are treated in steps of $0.1\lambda_c$, where λ_c is the free space wavelength at the center of the band, L_{λ_c} and a_{λ_c} are the normalized length and radius of the structure, respectively. That is, 1000 different geometries are simulated altogether—for each of the 3 tapering profiles. Note that some cases—for example, those with small length-to-radius ratios—are defined by a

combination of parameters that is unlikely to occur in nature and therefore are not realistic; nevertheless, these cases are included in the analysis for the sake of completeness. In this study, the trunk and the ground assume the following dielectric properties: the trunk has a homogeneous dielectric composition with a real part for the relative dielectric constant of $\varepsilon_{r,t}^{'} = 13.90$ and a conductivity of σ_t = 39 mS/m (specifically, these values correspond to an aspen tree trunk with 55% moisture content, as indicated by the measurement data appearing in Koubaa et al.);[15] and the ground has $\varepsilon_{r,g}^{'} = 5.45$ and σ_g = 20 mS/m (these values correspond to a soil with 8% clay, 30% sand, 62% silt, and 10% moisture content).[16,17]

3.1 Untapered Circular Cylindrical Trunk

The first case analyzed is the regular circular cylinder trunk model (Fig. 1a). Figures 2 and 3 show the average error in the analytical solution as referenced to the FDTD solution as functions of the trunk length, trunk radius, and incidence angle for the vv and hh responses. In order to limit the dynamic range of these error maps, error data points greater than 15 dB are simply set to 15 dB. A constant error contour is also extracted from each error map and is plotted in Figs. 4 and 5; here, the 3-dB error line is used, that is, if the trunk length and radius values lie in the region above this line, then the average error is expected to be less than 3 dB. (Note that for the vv response at θ_i = 15°, as the error does not fall below 3 dB for the region $a_{\lambda_c} > 0.2\lambda_c$ over the range of length values simulated, only a partial error line is drawn. For this special case, additional analysis of trunks with lengths up to $20\lambda_c$ is carried out; however, a complete error line still cannot be determined. The reasons for the poor accuracy are explained below.)

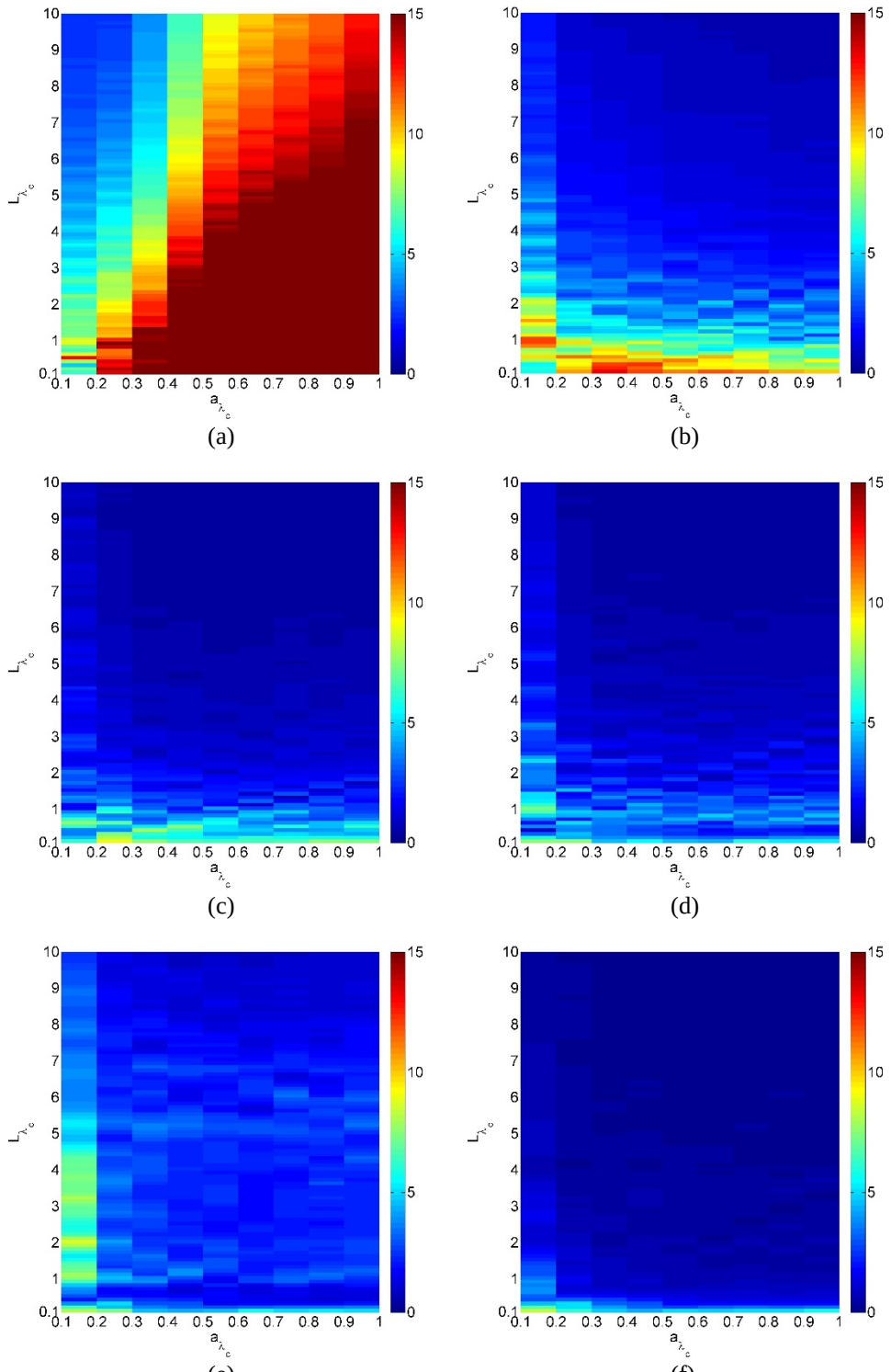

Fig. 2 Average error (in dB) in the vertical-vertical (vv) analytical solution for an untapered circular cylindrical tree trunk as functions of trunk length, trunk radius, and incidence angle: a) θ_i = 15°, b) θ_i = 30°, c) θ_i = 45°, d) θ_i = 60°, e) θ_i = 67°, and f) θ_i = 75°

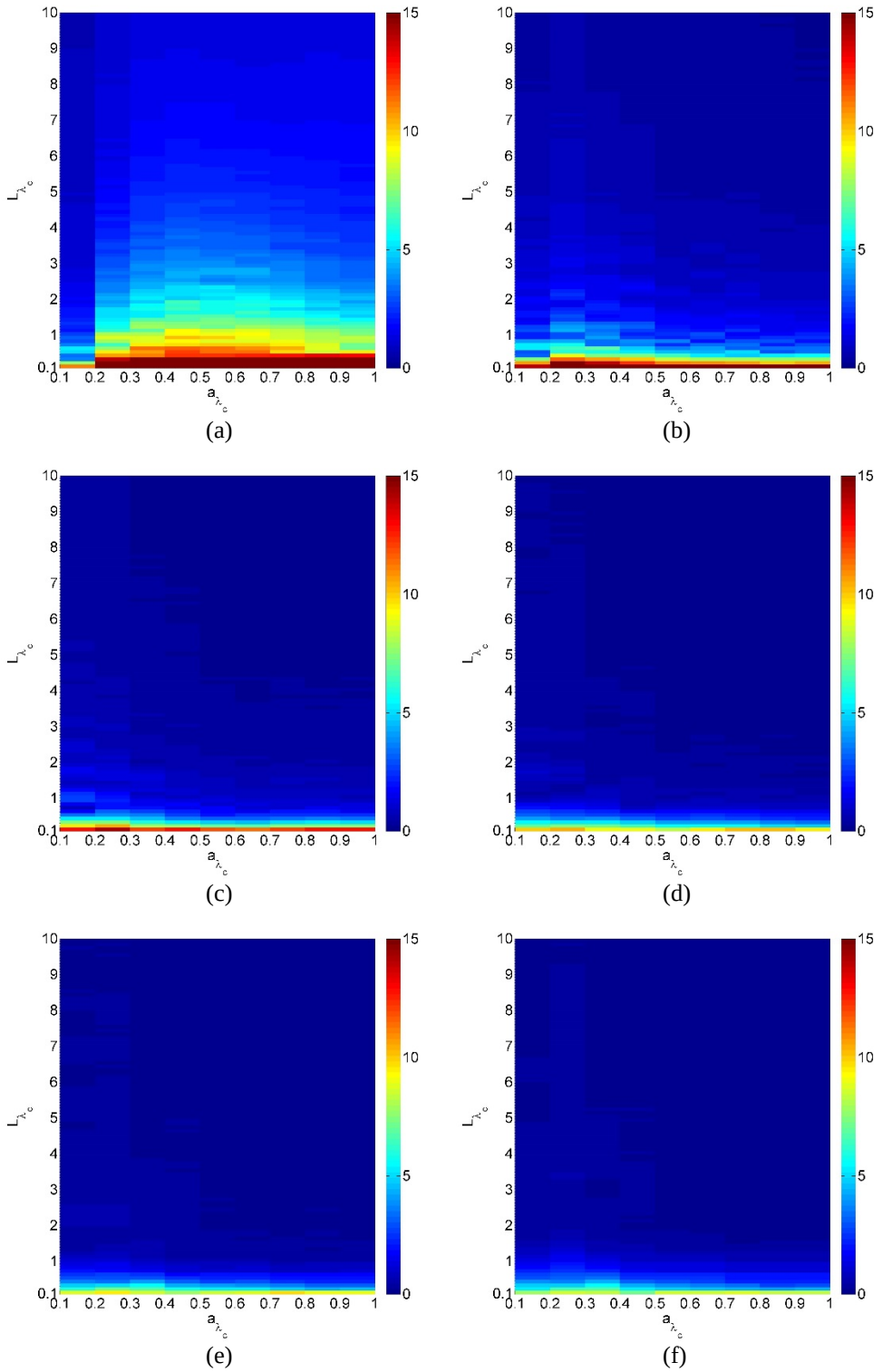

Fig. 3 Average error (in dB) in the horizontal-horizontal (hh) analytical solution for an untapered circular cylindrical tree trunk as functions of trunk length, trunk radius, and incidence angle: a) θ_i = 15°, b) θ_i = 30°, c) θ_i = 45°, d) θ_i = 60°, e) θ_i = 67°, and f) θ_i = 75°

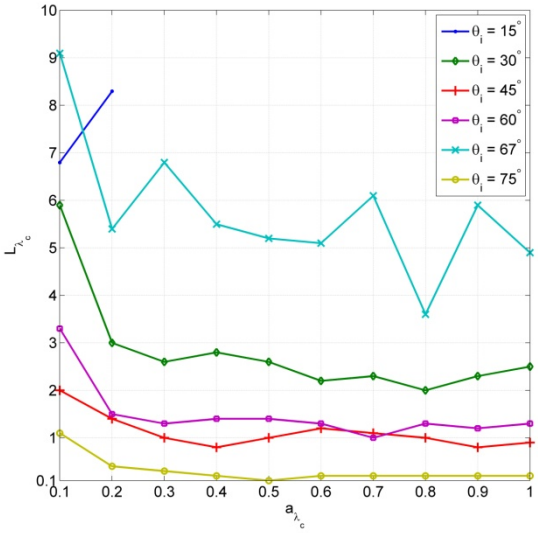

Fig. 4 The 3-dB error lines for an untapered circular cylindrical tree trunk as a function of incidence angle: vv solution

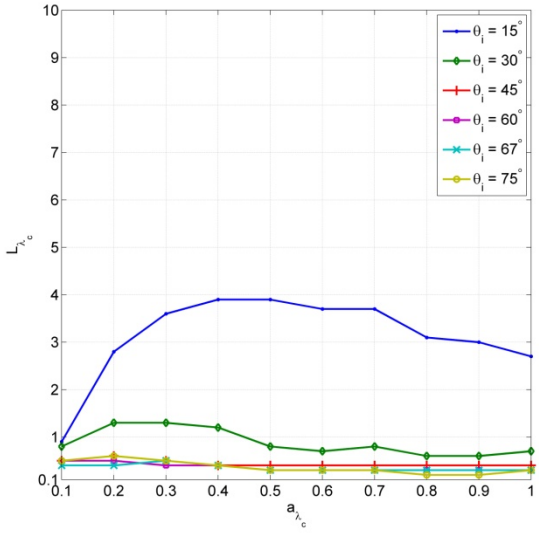

Fig. 5 The 3-dB error lines for an untapered circular cylindrical tree trunk as a function of incidence angle: hh solution

Figures 2 and 3 show that, for a given trunk radius, the error in the analytical solution in general decreases with increasing trunk length for both polarizations and at all incidence angles—albeit the error does not decrease in a monotonic fashion, especially for small length values, as evident by the non-smoothness of the intensity maps. The error profile of the vv solution as a function of the incidence angle is noticeably different from that of the hh solution owing to the Brewster angle effects. The range of validity of the hh solution is seen to improve as the incidence angle

increases, but there is an incidence angle beyond which the error maps remain relatively unchanged; here, that angle seems to occur at around $\theta_i = 45°$. In contrast, the vv solution tends to have larger errors at and near incidence angles at which the Brewster angle effects of the trunk and the ground come into play. In this case, the Brewster angles of the trunk and the ground are encountered at $\theta_i \approx 15°$ and $\theta_i \approx 67°$, respectively, and it is seen from Figs. 2a and 2e that the vv solution accuracy is degraded at those angles.

It should be noted that, in general, as the single ground-bounce returns become stronger (or more dominant) relative to the other scattering effects, the accuracy of the analytical solution tends to improve. This can be explained by the fact that the single ground-bounce responses essentially capture the scattering behavior of the trunk in the specular direction when the trunk is excited either directly by the incident wave or indirectly by a ground reflected wave.

From separate free space scattering simulations of the finite-length cylinder, it is seen that the volumetric current integration method is more accurate in modeling the specular scattering component than in capturing other effects such as scattering in the non-specular directions and scattering from the ends of the structure. (Specifically, the accuracy in the specular direction is better for hh than for vv, and improves with increasing length and incidence angle—with the exception that the vv case exhibits an error peak in the vicinity of the Brewster angle.) Therefore, in the presence of the ground, if strong single ground-bounce returns are established, then it can be expected that the analytical solution would be accurate. For the vv response at $\theta_i = 15°$, the poor accuracy of the analytical solution is due to the weakening of the single ground-bounce returns, the specular reflections from the trunk not being faithfully captured, and the fact that—especially as the radius increases—the backscattering component from the top and base of the trunk becomes stronger than or comparable to the single ground-bounce returns.

Note that, at least for vv, the analytical formulation better characterizes the backscattering component from the top and base of the trunk for small radius values than for large radius values; consequently, at $\theta_i = 15°$, the error increases with increasing radius for a given length; however, at other incidence angles, on average, the error tends to be smaller for larger radius values since the single ground-bounce returns are the more dominant responses relative to other effects. As it can be seen by juxtaposing Figs. 2a and 2e, the Brewster angle effect of the ground is not as detrimental as that of the trunk; at $\theta_i = 67°$, although the ground reflection is reduced, the finite-length cylinder approximation still better captures the specular reflections from the trunk at this angle than at $\theta_i = 15°$.

Overall, the error behavior of the hh solution exhibits less complexity as compared to that of the vv case. The hh backscattering solution has less than 3 dB of error as long as $L_{\lambda_c} > 4\lambda_c$ (Fig. 5), for the simulation parameters and range of radius and excitation angle values considered here. The stated criterion indicates the condition for which the hh-polarized, single ground-bounce returns are expected to be accurately modeled. It is also observed that in general the hh analytical solution may not always accurately account for the scattering from the top and base of the trunk, even for small radius values.

The usefulness of the error analysis conveyed by Figs. 2 through 5 notwithstanding, it is also instructive to examine the scattering characteristics in the imaging domain. The imaging response at pixel location $\vec{r}$, for a particular elevation observation angle θ_i, is obtained by averaging the backscattered responses over an aperture in azimuth as follows:

$$I_{pp}(\vec{r},\theta_i) = 4\pi\left|\frac{1}{N_{\phi_i}N_f}\sum_{\Delta\phi_i}\sum_{\Delta f} W_f(f)W_{\phi_i}(\phi_i)S_{pp}\left(-\hat{k}_i,\hat{k}_i\right)e^{j2k_o\hat{k}_i\cdot\vec{r}}\right|^2, \; pp = vv, hh \tag{4}$$

where $\Delta\phi_i$ is the extent of the observation aperture, N_{ϕ_i} is the number of observation angles, $W_{\phi_i}(\phi_i)$ is the window in azimuth, and $W_f(f)$ is the window in the frequency domain. In this work, only the imaging response on the ground plane is considered.

Comparisons of the FDTD solution-based and analytical solution-based images for a few representative examples are shown in Figs. 6 and 7, for vv and hh, respectively. These examples are chosen from regions where the average error of the analytical solution in the frequency domain is expected to be less than 3 dB.

In all cases, the observation aperture is centered at ϕ_i = 0°, with $\Delta\phi_i \approx 49°$, $N_{\phi_i} = 49$, Δf = [200 MHz, 500 MHz], and N_f = 301; and the base of the trunk is centered at the origin.

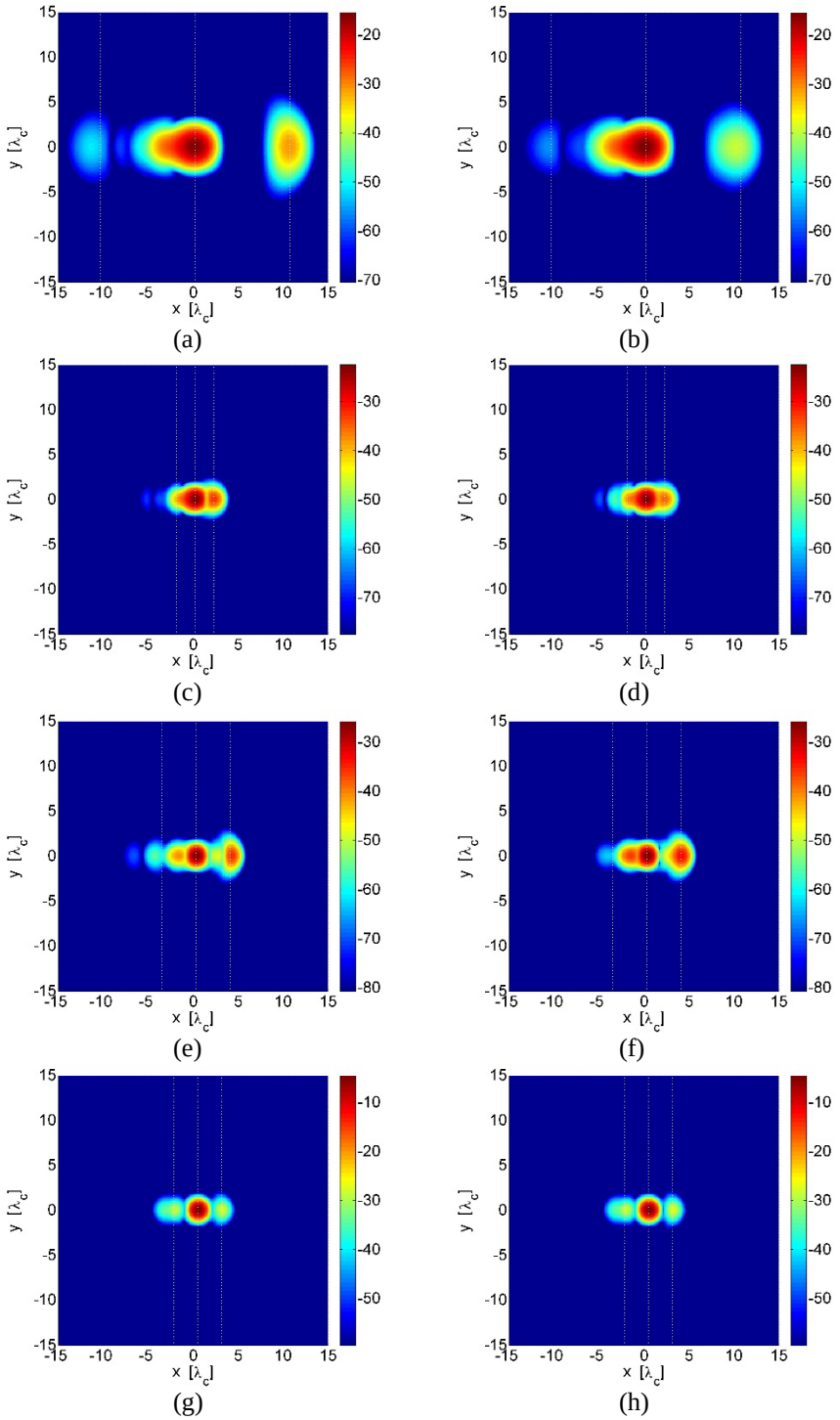

Fig. 6 Imaging response (vv) of an untapered circular cylindrical tree trunk, full-wave solution (left) vs. analytical solution (right): a–b) $\theta_i = 30°$, $L_{\lambda_c} = 6.1$, $a_{\lambda_c} = 0.2$**; c–d)** $\theta_i = 60°$, $L_{\lambda_c} = 3.6$, $a_{\lambda_c} = 0.2$**; e–f)** $\theta_i = 67°$, $L_{\lambda_c} = 9.0$, $a_{\lambda_c} = 0.3$**; and g–h)** $\theta_i = 75°$, $L_{\lambda_c} = 10.0$, $a_{\lambda_c} = 0.5$

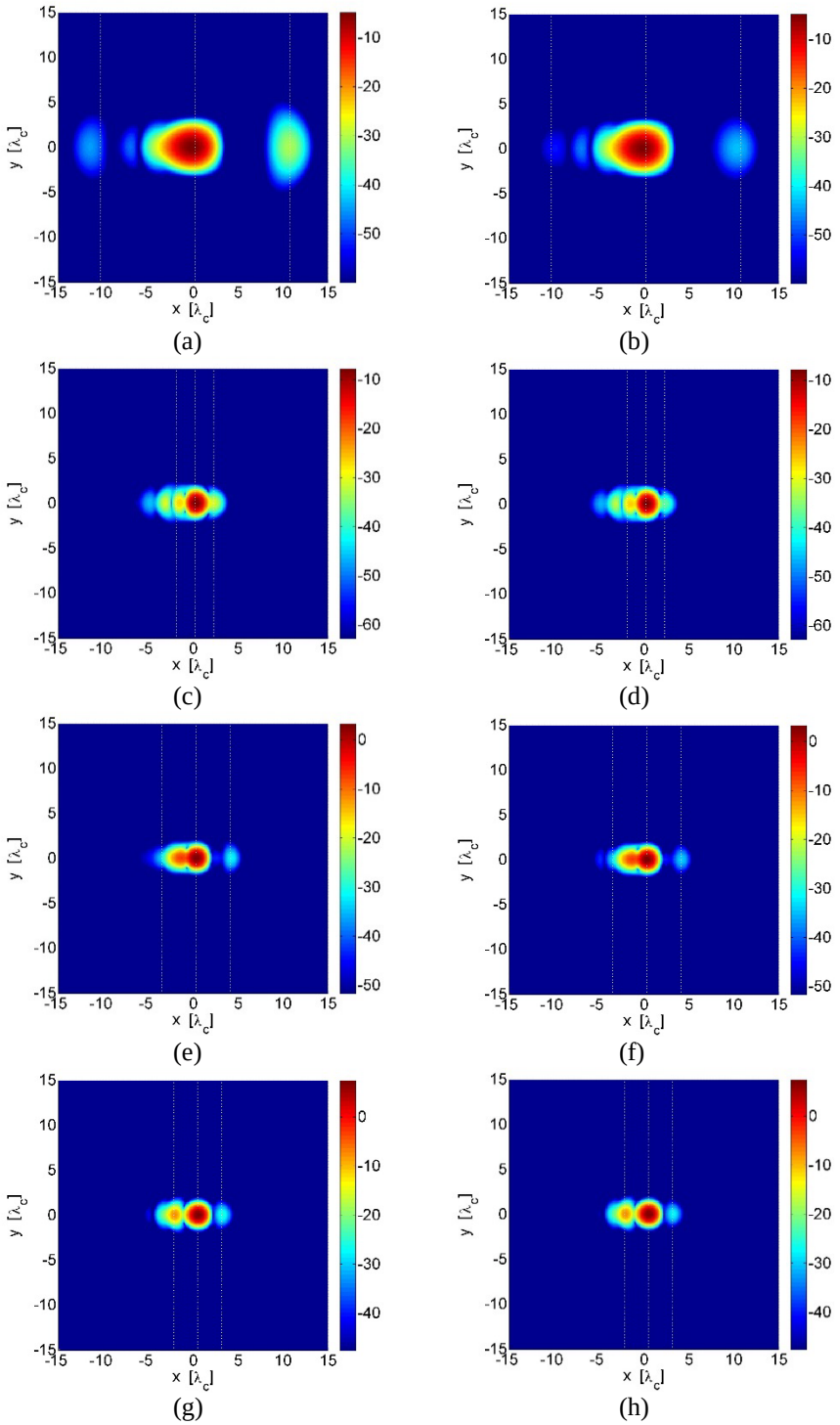

Fig. 7 Imaging response (hh) of an untapered circular cylindrical tree trunk, full-wave solution (left) vs. analytical solution (right): a–b) $\theta_i = 30°$, $L_{\lambda_c} = 6.1$, $a_{\lambda_c} = 0.2$; **c–d)** $\theta_i = 60°$, $L_{\lambda_c} = 3.6$, $a_{\lambda_c} = 0.2$; **e–f)** $\theta_i = 67°$, $L_{\lambda_c} = 9.0$, $a_{\lambda_c} = 0.3$; **and g–h)** $\theta_i = 75°$, $L_{\lambda_c} = 10.0$, $a_{\lambda_c} = 0.5$

As seen from the results, the most identifiable features in the images come from the following: 1) the scattering from the top of the trunk, 2) the single ground-bounce (dihedral) returns, and 3) the double ground-bounce response of the top of the trunk (that is, the subsurface mirror term of the scattering from the top of the trunk). These are referred to as the lower-order effects, with the single ground-bounce terms generating the dominant effect as the length of the trunk increases. Note that the scattering from the base of the trunk produces imaging responses that coincide with the single ground-bounce responses. Of course, there are higher-order (less prominent, less readily identifiable) effects embedded in the scattering data: these consist of higher-order ground bounces, as well as effects produced by, for example, internal bounces within the cylinder, multiple end-to-end bounces, creeping waves, and various combinations of interactions among the above modes. It can be shown that the down-range locations of the 3 lower-order scattering features are $x_1 \approx a_{\lambda_c} + L_{\lambda_c} / \tan\theta_i$, $x_2 \approx a_{\lambda_c}$, and $x_3 \approx a_{\lambda_c} - L_{\lambda_c} / \tan\theta_i$; these locations are marked in the images by dotted vertical lines from right to left.

The images demonstrate that the single ground-bounce returns are accurately modeled by the analytical solution; the scattering from the top of the trunk, the double ground-bounce return, and higher-order effects, on the other hand, may not be captured as consistently, or as accurately. In general, considering the imaging response as a whole, the match between the numerical and the analytical solutions tends to improve as the trunk length increases.

3.2 Linearly Tapered Circular Cylindrical Trunk

For a cone-shaped tree trunk (Fig. 1b), the trunk-ground dihedral effect is reduced. In other words, the single ground-bounce returns do not contain the direct specular reflection interactions with the trunk that define the error behavior of the untapered case. However, when the cone length is large relative to the base radius, the interactions with the structure are such that a scattering component in a direction close to specular is established in the single ground-bounce returns.

Error maps are first generated as before; however, for space considerations, these maps are not explicitly included here. Instead, only their 3-dB error lines are presented, as displayed in Figs. 8 and 9. Comparing Figs. 5 and 9 for the hh response, it is seen that the error behaviors for the untapered and linearly tapered geometries do not differ significantly. The most noticeable difference between the 2 cases is that, for a fixed length value, the error tends to increase with increasing base radius for the cone. This behavior—more evident for small length values—is attributable to the fact that as the base radius increases, the single ground-bounce returns contain interactions with the cone that are farther from specular.

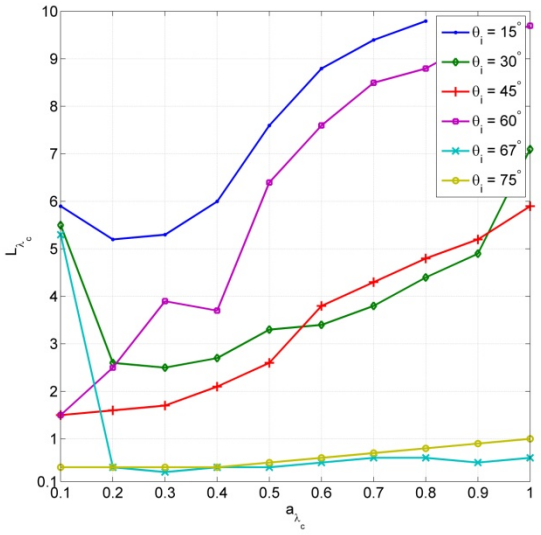

Fig. 8 The 3-dB error lines for a linearly tapered circular cylindrical tree trunk as a function of incidence angle: vv solution

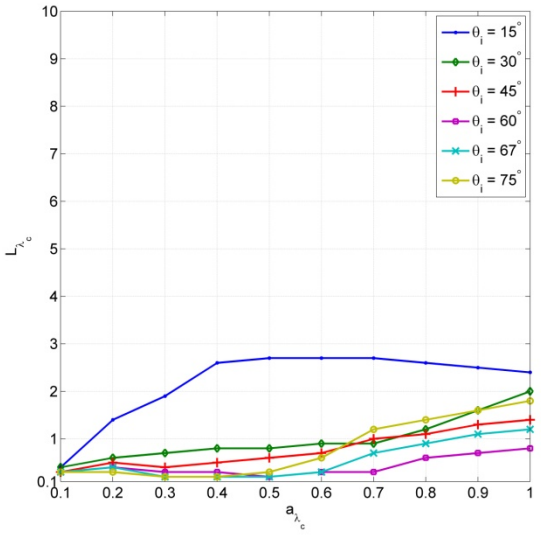

Fig. 9 The 3-dB error lines for a linearly tapered circular cylindrical tree trunk as a function of incidence angle: hh solution

The influence of the Brewster angle effects of the trunk and the ground on the vv solution error is more complicated than that observed for the untapered geometry, since here the slant angle of the side of the trunk is dependent on the length-to-base radius ratio. Relative to the Brewster angle effects, the single ground-bounce returns' non-specular interactions with the trunk are seen to be the more important factor in determining the validity of the analytical solution. As a result, as illustrated in Fig. 8 (for θ_i = 30°, 45°, 60°, and 75°), the region of validity of the solution for

the cone is reduced compared to that for the untapered cylinder; the error, for a fixed length value, also mostly increases with increasing radius for the same reason mentioned above for the hh case. Note that, relative to the single ground-bounce returns, the scattering component from the top of the cone is weaker than the one from the top of the regular cylinder, as expected. For the vv case, this leads to better accuracy (larger region of validity) at θ_i = 15° and 67° for the cone, as shown in Fig. 8.

Next, images are generated for an example set with the same parameters as those considered in the preceding section for the regular cylinder. The results are displayed in Figs. 10 and 11, and show that the single ground-bounce components are accurately reproduced by the analytical solution. Comparing the images with those for the regular cylinder case, the distinctive feature here is that the response from the top of the structure and its double ground-bounce return have been significantly reduced (relative to the main response); this is reflected in both the numerical and analytical solutions. (Note that it is not appropriate to make a direct comparison of the amplitudes of the image responses between the regular cylinder and cone cases here, since for the same length and radius values, the 2 structures have different volumes.)

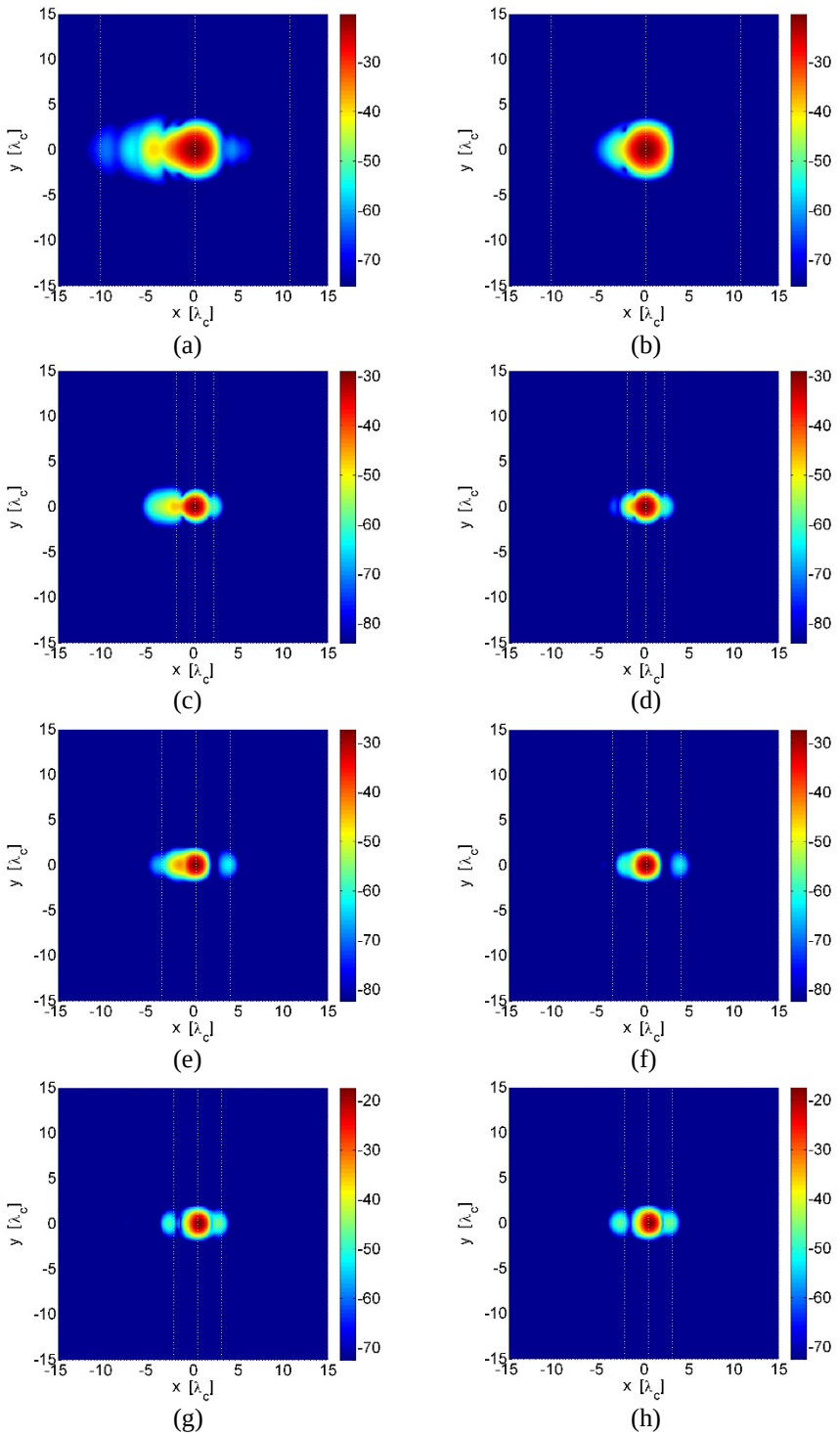

Fig. 10 Imaging response (vv) of a linearly tapered circular cylindrical tree trunk, full-wave solution (left) vs. analytical solution (right): a–b) $\theta_i = 30°$, $L_{\lambda_c} = 6.1$, $a_{\lambda_c} = 0.2$; **c–d)** $\theta_i = 60°$, $L_{\lambda_c} = 3.6$, $a_{\lambda_c} = 0.2$; **e–f)** $\theta_i = 67°$, $L_{\lambda_c} = 9.0$, $a_{\lambda_c} = 0.3$; **and g–h):** $\theta_i = 75°$, $L_{\lambda_c} = 10.0$, $a_{\lambda_c} = 0.5$

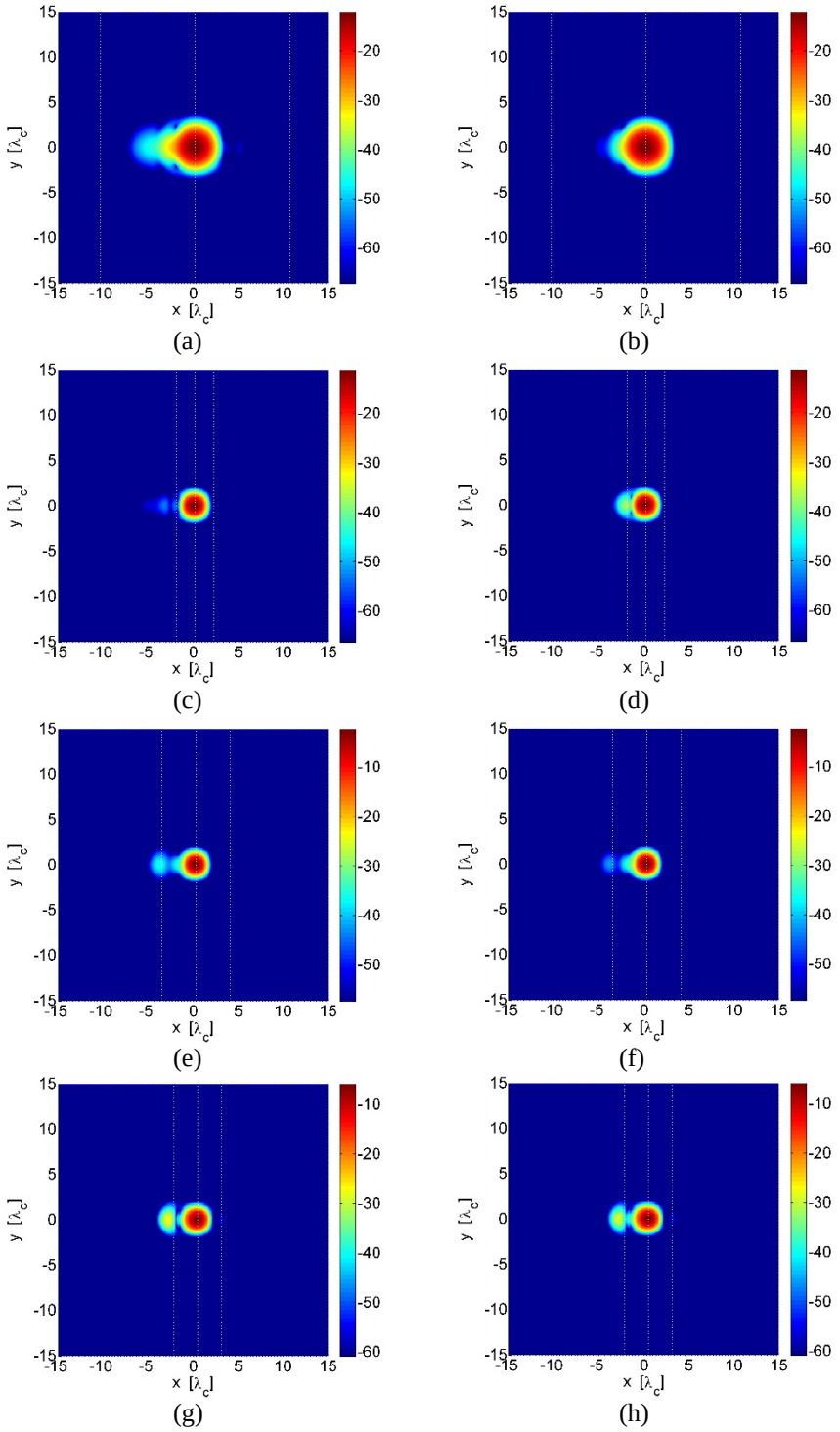

Fig. 11 Imaging response (hh) of a linearly tapered circular cylindrical tree trunk, full-wave solution (left) vs. analytical solution (right): a–b) $\theta_i = 30°$, $L_{\lambda_c} = 6.1$, $a_{\lambda_c} = 0.2$; **c–d)** $\theta_i = 60°$, $L_{\lambda_c} = 3.6$, $a_{\lambda_c} = 0.2$; **e–f)** $\theta_i = 67°$, $L_{\lambda_c} = 9.0$, $a_{\lambda_c} = 0.3$; **and g–h)** $\theta_i = 75°$, $L_{\lambda_c} = 10.0$, $a_{\lambda_c} = 0.5$

3.3 Nonlinearly Tapered Circular Cylindrical Trunk

The trunk geometry examined next is akin to a cone structure with an exponential expansion near its base. The tapering profile shown in Fig. 1c is generated by following the procedure outlined by Weber and Penn[11] using the parameters *nTaper* = 1 and *Flare* = 0.6. As mentioned, such a profile with a slightly flared base is expected to provide a closer emulation of trunk geometries encountered in nature.

Only the 3-dB error lines for the analytical solution are included, as shown in Figs. 12 and 13. The plots are similar to those for the cone structure. It is seen that the presence of the flare does not significantly change the error behavior. The observations presented previously for the cone are equally applicable here. (Note that, as shown by Weber and Penn,[11] by changing the *nTaper* and *Flare* parameters, a variety of trunk profiles can be generated; the values used here are expected to be adequate for the types of trees treated in this study.)

Images for trunks with the above tapering profile are illustrated in Figs. 14 and 15—for the same example set considered in the previous 2 sections. Good agreement between the numerical and analytical solutions is seen—though, once again, the single ground-bounce returns are more accurately reproduced than other less prominent scattering effects. Overall, the results demonstrate that the discrete cylinder model can be an acceptable approach for analyzing a trunk with non-constant radius along its length.

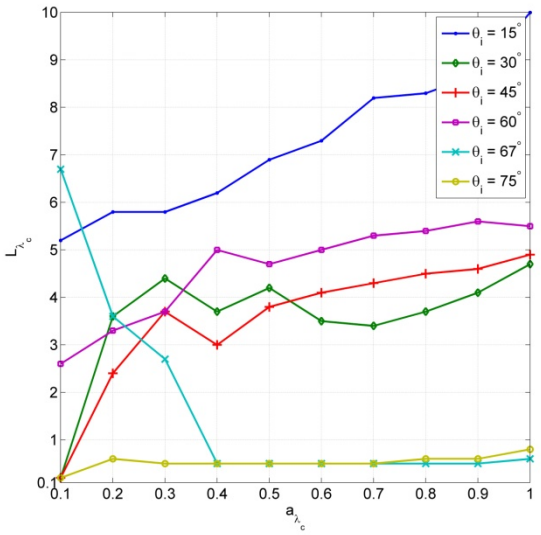

Fig. 12 The 3-dB error lines for a nonlinearly tapered circular cylindrical tree trunk as a function of incidence angle: vv solution

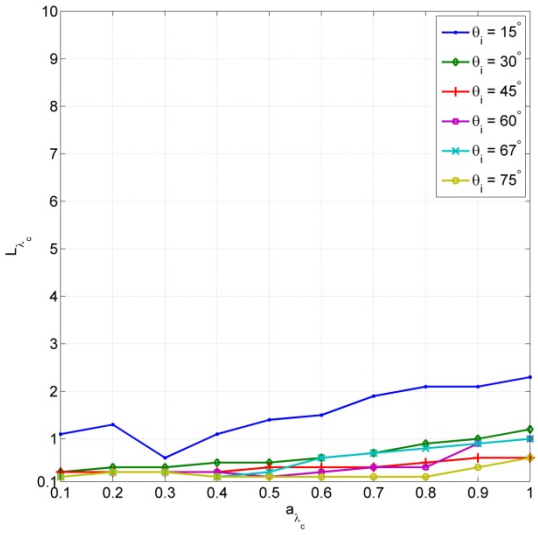

Fig. 13 The 3-dB error lines for a nonlinearly tapered circular cylindrical tree trunk as a function of incidence angle: hh solution

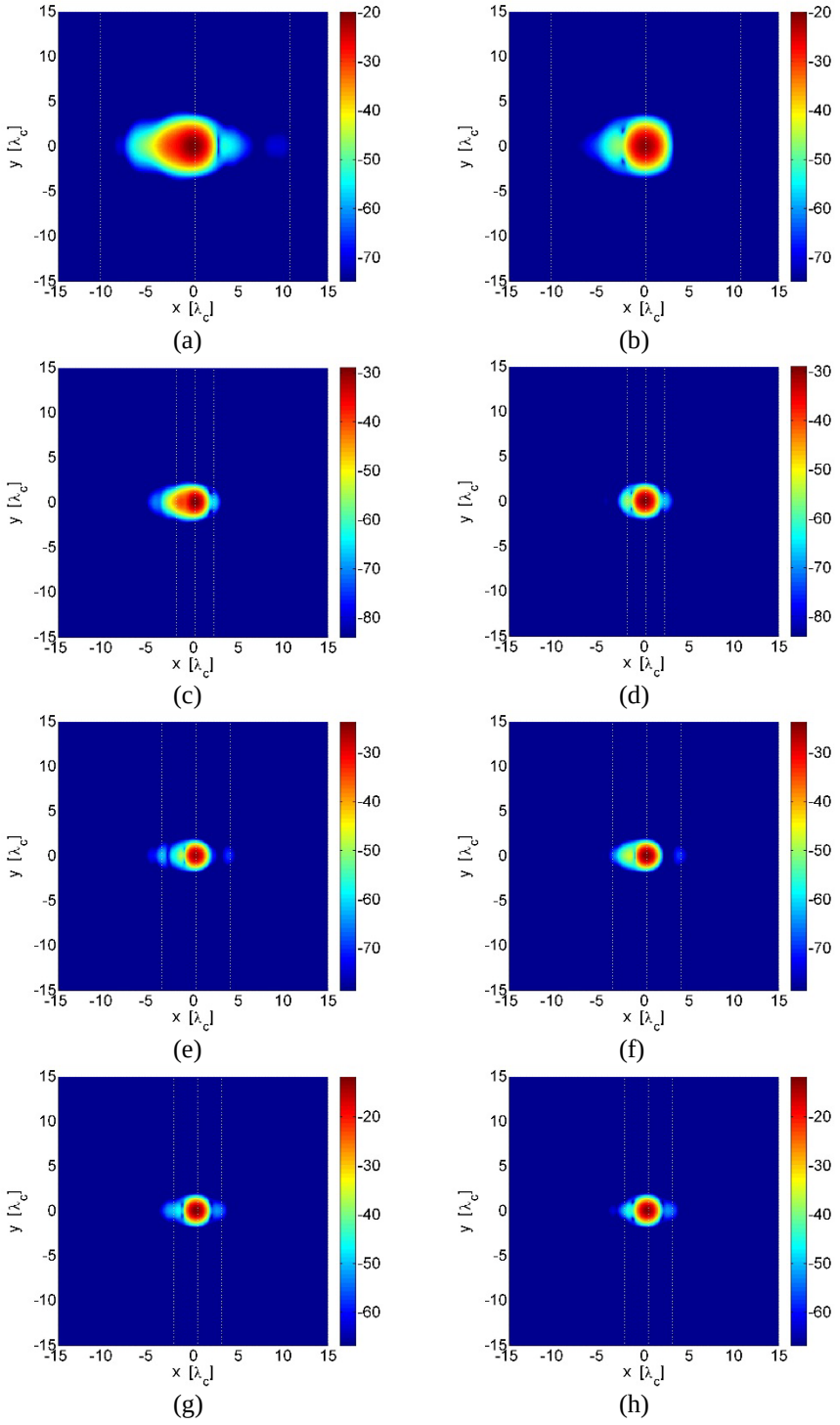

Fig. 14 Imaging response (vv) of a nonlinearly tapered circular cylindrical tree trunk, full-wave solution (left) vs. analytical solution (right): a–b) $\theta_i = 30°$, $L_{\lambda_c} = 6.1$, $a_{\lambda_c} = 0.2$; **c–d)** $\theta_i = 60°$, $L_{\lambda_c} = 3.6$, $a_{\lambda_c} = 0.2$; **e–f)** $\theta_i = 67°$, $L_{\lambda_c} = 9.0$, $a_{\lambda_c} = 0.3$; **and g–h)** $\theta_i = 75°$, $L_{\lambda_c} = 10.0$, $a_{\lambda_c} = 0.5$

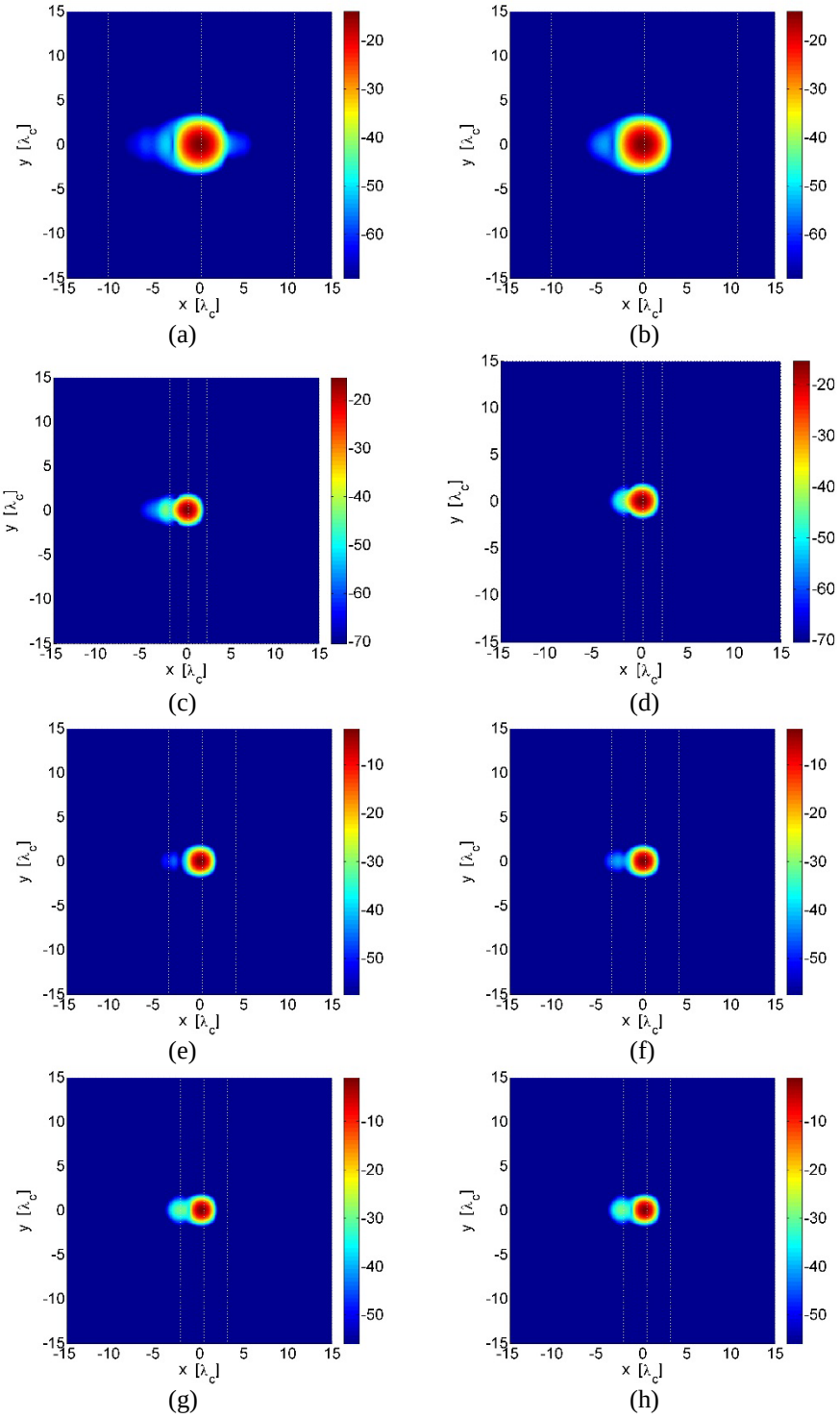

Fig. 15 Imaging response (hh) of a nonlinearly tapered circular cylindrical tree trunk, full-wave solution (left) vs. analytical solution (right): a–b) $\theta_i = 30°$, $L_{\lambda_c} = 6.1$, $a_{\lambda_c} = 0.2$**; c–d)** $\theta_i = 60°$, $L_{\lambda_c} = 3.6$, $a_{\lambda_c} = 0.2$**; e–f)** $\theta_i = 67°$, $L_{\lambda_c} = 9.0$, $a_{\lambda_c} = 0.3$**; and g–h)** $\theta_i = 75°$, $L_{\lambda_c} = 10.0$, $a_{\lambda_c} = 0.5$

4. Conclusions

The accuracy of the volumetric current integration method for characterizing the backscattering response of a tree trunk located above a dielectric ground is investigated. The region of validity of the analytical solution—as functions of trunk length, trunk radius, incidence angle, polarization, and trunk tapering—is determined by comparing the frequency-domain results to those from a full-wave method. It is noted that the vv solution is, in general, valid over a smaller range of length and radius values than the hh solution, as a result of the Brewster angle effects of the trunk and the ground. The range of validity is also negatively impacted—albeit less so for hh than for vv—by the presence of tapering, a feature that results in single ground bounces defined by non-specular interactions with the trunk. It is observed that for both the untapered and tapered profiles, the range of validity of the 2 co-polarized responses becomes comparable as the incidence angle approaches grazing. To demonstrate the practicality of the formulations and observations, monostatic images of the tree trunks are also constructed. Comparisons with numerical solution-based images indicate that while the analytical solution can correctly model the single ground-bounce returns, it may not consistently capture other less prominent effects such as, for example, scattering from the top of the structure and higher-order interactions.

5. References

1. Liao DH, Dogaru T. Large-Scale, Full-wave scattering phenomenology characterization of realistic trees. Proc. IEEE Antennas and Propagation Symposium, 2015.
2. Sarabandi K, Koh I-S. Full-wave simulation of propagation channel parameters for a forest environment. Proc. IEEE Antennas and Propagation Symposium, 2000.
3. Lang RH, Sidhu JS. Electromagnetic backscattering from a layer of vegetation: a discrete approach. IEEE Trans Geosci Rem Sens. 1983;21(1):62–71.
4. Seker S, Schneider A. Electromagnetic scattering from a dielectric cylinder of finite length. IEEE Trans Antennas and Propagation. 1988;36:303–307.
5. Karam MA, Fung AK, Antar YMM. Electromagnetic wave scattering from some vegetation samples. IEEE Trans Geosci Rem Sens. 1988;26(6):799–808.
6. Ulaby FT, Elachi C, editors. Radar polarimetry for geoscience applications. Norwood (MA): Artech House; 1990.
7. Lang RH, de Matthaeis P. Comparison of surface and volume currents models for electromagnetic scattering from finite dielectric cylinders. IEEE Trans Antennas and Propagation. 2009;57(7):2216–2220.
8. Liao DH. Scattering from the finite-length, dielectric circular cylinder: part i--derivation of an analytical solution. Adelphi (MD): Army Research Laboratory (US); 2015. Report No.: ARL-TR-7346.
9. Thirion L, Chênerie I, Dahon C, Ferro-Famil L, Lefevre A, Titin-Schnaider C. Modelling of the scattering by a smooth dielectric cylinder: Study of the complex scattering matrix using two different models, presented at the ESA Polinsar 2003 Workshop, 2003.
10. Lang RH, de Matthaeis P. Microwave scattering models for cylindrical vegetation components. Progress In Electromagnetics Research. 2005;55:307–333.
11. Weber J, Penn J. Creation and rendering of realistic trees. Proc. Int. Conf. Comput. Graph. Interactive Tech. 1995.
12. Lopez-Sanchez JM, Esteban-Gonzalez H, Baquero-Escudero M, Fortuny-Guasch J. An electromagnetic scattering model for multiple tree trunks above a tilted rough ground plane. IEEE Trans Geoscience and Remote Sensing. 1999;37(2):659–667.

13. Dogaru T, Le C. SAR images of rooms and buildings based on FDTD computer models. IEEE Trans. Geosci. and Remote Sens. 2009;47(5):1388–1401.

14. Liao DH, Dogaru T. Full-wave characterization of rough terrain surface scattering for forward-looking radar applications. IEEE Trans. Antennas and Propagat. 2012;60(8):3853–3866.

15. Koubaa A, Perré P, Hutcheon RM, Lessard J. Complex Dielectric Properties of the Sapwood of Aspen, White Birch, Yellow Birch, and Sugar Maple. Drying Technology. 2008;26(5):568–578.

16. Peplinski NR, Ulaby FT, Dobson MC. Dielectric properties of soils in the 0.3-1.3-GHz range. IEEE Trans Geoscience and Remote Sensing. 1995;33(3):803–807.

17. Dobson MC, Ulaby FT, Hallikainen MT, El-Rayes MA. Microwave dielectric behavior of wet soil—part ii: dielectric mixing models. IEEE Trans Geoscience and Remote Sensing. 1985;23(1):35–46.

Appendix. Scattering Solution for the Finite-Length, Dielectric Circular Cylinder in Free Space

Formulations from Part I of this study[8] are included here for convenience. The free space scattering matrix elements of a finite-length, dielectric circular cylinder with length L, radius a, and complex relative dielectric constant $\varepsilon_{r,t}$ are derived as

$$S_{pq}^{fs}\left(\hat{k}_s,\hat{k}_i\right)=\hat{p}_s\cdot\frac{k_o^2\left(\varepsilon_{r,t}-1\right)L}{2}\operatorname{sinc}\left(\frac{k_oL\left(\cos\theta_i+\cos\theta_s\right)}{2}\right)\sum_{n=-\infty}^{+\infty}\left[\vec{\mathrm{K}}_{1,n}+\vec{K}_{2,n}+\vec{K}_{3,n}\right]e^{jn\left(\phi_s-\phi_i\right)},\ p,q=v,h \tag{A-1}$$

where

$$\vec{\mathrm{K}}_{1,n}=\frac{jk_oI_{n+1}e^{j\phi_s}}{2k_{\rho,r}}\left(\beta_n-j\alpha_n\right)\left(\hat{x}-j\hat{y}\right);\ \vec{\mathrm{K}}_{2,n}=-\frac{jk_oI_{n-1}e^{-j\phi_s}}{2k_{\rho,r}}\left(\beta_n+j\alpha_n\right)\left(\hat{x}+j\hat{y}\right);\ \vec{\mathrm{K}}_{3,n}=I_n\gamma_n\hat{z}$$

. (A-2)

For $q = v$,

$$\alpha_n=\frac{jM_n\sin\theta_i\cos\theta_i}{J_n\left(k_{\rho,r}a\right)R_n};\quad \beta_n=\frac{nW\sin\theta_i\cos\theta_i}{J_n\left(k_{\rho,r}a\right)R_n};\quad \gamma_n=\frac{jM_n\sin\theta_i}{J_n\left(k_{\rho,r}a\right)R_n}; \tag{A-3}$$

for $q = h$,

$$\alpha_n=\frac{-nW\sin\theta_i\cos^2\theta_i}{J_n\left(k_{\rho,r}a\right)R_n};\quad \beta_n=\frac{jN_n\sin\theta_i}{J_n\left(k_{\rho,r}a\right)R_n};\quad \gamma_n=\frac{-nW\sin\theta_i\cos\theta_i}{J_n\left(k_{\rho,r}a\right)R_n}; \tag{A-4}$$

and

$$I_n=\frac{a^2}{\left(k_{\rho,r}a\right)^2-\left(k_{\rho,s}a\right)^2}\left(k_{\rho,r}aJ_n\left(k_{\rho,s}a\right)J_{n+1}\left(k_{\rho,r}a\right)-k_{\rho,s}aJ_n\left(k_{\rho,r}a\right)J_{n+1}\left(k_{\rho,s}a\right)\right); \tag{A-5}$$

$$R_n=\frac{\pi\left(k_{\rho,i}a\right)^2H_n^{(2)}\left(k_{\rho,i}a\right)}{2}\cdot\left[M_n\cdot N_n-W^2n^2\cos^2\theta_i\right]; \tag{A-6}$$

$$M_n=\frac{H_n^{(2)}{}'\left(k_{\rho,i}a\right)}{k_{\rho,i}aH_n^{(2)}\left(k_{\rho,i}a\right)}-\frac{J_n{}'\left(k_{\rho,r}a\right)}{k_{\rho,r}aJ_n\left(k_{\rho,r}a\right)}; \tag{A-7}$$

$$N_n=\frac{H_n^{(2)}{}'\left(k_{\rho,i}a\right)}{k_{\rho,i}aH_n^{(2)}\left(k_{\rho,i}a\right)}-\varepsilon_{r,t}\frac{J_n{}'\left(k_{\rho,r}a\right)}{k_{\rho,r}aJ_n\left(k_{\rho,r}a\right)}; \tag{A-8}$$

$$W=\frac{1}{\left(k_{\rho,i}a\right)^2}-\frac{1}{\left(k_{\rho,r}a\right)^2}. \tag{A-9}$$

The above assumes $k_{\rho,i} = k_o \sin\theta_i$, $k_{\rho,s} = k_o \sin\theta_s$, $k_{\rho,r} = k_o\sqrt{\varepsilon_{r,t} - \cos^2\theta_i}$, and that the incident and scattered wave directions ($\hat{k}_i$, $\hat{k}_s$) and their associated polarization vectors ($\hat{h}$, $\hat{v}$) are defined by

$$\hat{k}_i = \sin\theta_i \cos\phi_i \hat{x} + \sin\theta_i \sin\phi_i \hat{y} - \cos\theta_i \hat{z}\,; \tag{A-10}$$

$$\hat{k}_s = \sin\theta_s \cos\phi_s \hat{x} + \sin\theta_s \sin\phi_s \hat{y} + \cos\theta_s \hat{z}\,; \tag{A-11}$$

$$\hat{h}_{i,s} = \frac{\hat{z} \times \hat{k}_{i,s}}{\left|\hat{z} \times \hat{k}_{i,s}\right|}\,; \tag{A-12}$$

$$\hat{v}_{i,s} = \hat{h}_{i,s} \times \hat{k}_{i,s}\,; \tag{A-13}$$

in which the subscripts *i* and *s* identify quantities related to the incident and scattered waves, respectively; θ_i is the incidence angle in elevation (measured from - $\hat{z}$); θ_s is the scattering angle in elevation (measured from + $\hat{z}$); and $\phi_{i,s}$ is the incidence/scattering angle in azimuth (measured from + $\hat{x}$).

1 (PDF) DEFENSE TECHNICAL INFORMATION CTR DTIC OCA

2 (PDF) DIRECTOR US ARMY RESEARCH LAB RDRL CIO LL IMAL HRA MAIL & RECORDS MGMT

1 (PDF) GOVT PRINTG OFC A MALHOTRA

5 (PDF) DIRECTOR US ARMY RESEARCH LAB RDRL SER T DOGARU C KENYON C LE D LIAO A SULLIVAN